Chromatin loading of MCM hexamers is associated with di-/tri-methylation of histone H4K20 toward S phase entry

Yoko Hayashi-Takanaka[1,*], Yuichiro Hayashi[2], Yasuhiro Hirano[1], Atsuko Miyawaki-Kuwakado[3], Yasuyuki Ohkawa[3], Chikashi Obuse[4], Hiroshi Kimura[5], Tokuko Haraguchi[1] and Yasushi Hiraoka[1,*]

[1] Graduate School of Frontier Biosciences, Osaka University, 1-3 Yamadaoka, Suita 565-0871, Japan

[2] Institute of Biomedical Sciences, Kansai Medical University, 2-5-1 Shin-machi, Hirakata 573-1010, Japan

[3] Division of Transcriptomics, Medical Institute of Bioregulation, Kyushu University, 3-1-1 Maidashi, Higashi-ku, Fukuoka 812-0054, Japan

[4] Department of Biological Sciences, Graduate School of Science, Osaka University, 1-1 Machikaneyama, Toyonaka 560-0043, Japan

[5] Cell Biology Center, Institute of Innovative Research, Tokyo Institute of Technology, 4259 Nagatsuta, Midori-ku, Yokohama 226-8503, Japan

[*]Correspondence should be addressed to:
Yoko Hayashi-Takanaka
Graduate School of Frontier Biosciences, Osaka University, 1-3, Yamadaoka, Suita, 565-0871, Japan
E-mail: ythayashi@fbs.osaka-u.ac.jp
or
Yasushi Hiraoka,
Graduate School of Frontier Biosciences, Osaka University, 1-3, Yamadaoka, Suita, 565-0871, Japan
E-mail: hiraoka@fbs.osaka-u.ac.jp

Abstract

Replication of genomic DNA is a key step in initiating cell proliferation. Loading hexameric complexes of minichromosome maintenance (MCM) helicase on DNA replication origins during the G1 phase is essential in initiating DNA replication. Here, we show that stepwise loading of two hexamer complexes of MCM occurs during G1 progression in human cells. This transition from the single-to-double hexamer was associated with levels of methylation at lysine 20 of histone H4 (H4K20). A single hexamer of MCM complexes was loaded at the replication origins with the presence of H4K20 monomethylation (H4K20me1) in the early G1 phase, then another single hexamer was recruited to form a double hexamer later in G1 as H4K20me1 was converted to di-/tri-methylation (H4K20me2/me3). Under non-proliferating conditions, cells stay halted at the single-hexamer state in the presence of H4K20me1. We propose that the single-hexamer state on chromatin is a limiting step in making the proliferation-quiescence decision.

Introduction

Replication of genomic DNA is crucial for the proliferation of living organisms. The G1 phase of the cell cycle is an important step in preparation for DNA replication in the S phase (1,2). During the G1 phase, mammalian cells decide either to enter the S phase for proliferation or halt at the G1 phase for quiescence (3). While most cancer cells lose the ability to be arrested at the G1 phase, normal cells are typically arrested in the G1 phase in response to accumulation of DNA damage or external stimuli, resulting in a prolonged cell cycle (4). Once the cells pass through the G1 checkpoint, they enter the S phase in 2–4 h, with no need for other stimuli (5). Therefore, the decision to exit the G1 phase is a key event in entering the S phase for cell proliferation.

Prior to the S phase, the assembly of the "pre-replication complex" (pre-RC) at DNA replication origins on chromatin is an essential step during the G1 phase ((6,7) reviewed in (8-10)). This complex consists of the origin recognition complex (ORC), Cdc6, Cdt1, and minichromosome maintenance protein (MCM). By the end of the G1 phase, two copies of the MCM hexamer (Mcm2-7) are loaded on the replication origin to function as a DNA helicase in the S phase. Metazoan replication origins do not share a clear consensus sequence, although they tend to have enriched GC-rich sequences and G4 quadruplex structures (11,12). In contrast, in the budding yeast *Saccharomyces cerevisiae*, an autonomously replicating sequence (ARS) containing the replication origin has been identified (13,14). *In vitro* studies using recombinant yeast proteins showed that Orc1-6, Cdc6, Cdt1, and Mcm2-7 are sufficient for pre-RC assembly on the replication origin (15,16). Two hexamer complexes of MCM are sequentially loaded on chromatin: first, a single MCM hexamer is recruited to the replication origin where the ORC complex had already been loaded with the help of Cdc6 and Cdt1 (17,18); then, a second MCM

hexamer is loaded to form a double MCM hexamer. Structures of the single and double MCM hexamers and their intermediates are also determined using *in vitro* reconstituted complexes of recombinant yeast proteins by cryo-electron microscopy (19,20). In mammalian cells, however, it is still unknown when and how single and double MCM hexamers are formed *in vivo* on chromatin in the G1 phase. In addition, the chromatin state required for MCM hexamer formation remains to be elucidated.

Chromatin features, such as histone modifications, are also involved in replication initiation (21). Lysine 20 of histone H4 (H4K20) is a major methylated residue on the histone H4 tail that can exist in the mono-, di-, and tri-methylation forms (H4K20me1, H4K20me2, and H4K20me3, respectively). H4K20 methylation is involved in DNA replication, including the initiation step and maintenance of genome integrity (22), and H4K20me2 and H4K20me3, which are methylated from H4K20me1 by Suv420h1 and Suv420h2 (also called KMT5B and KMT5C, respectively), serve as binding sites for mammalian Orc1 and its cofactors (23,24). Moreover, the histone methyltransferase Set8 (also known as KMT5A or PR-set7), which catalyzes monomethylation of histone H4 at K20, limits the recruitment of Orc1 and MCM to chromatin in the G1 phase (25) through Set8-dependent regulation of chromatin compaction (26). Therefore, the regulation of histone H4K20 by Set8 and/or Suv420h1/2 methyltransferase is crucial for the pre-RC assembly on chromatin during the G1 phase to initiate DNA replication.

Here, we studied the MCM assembly on chromatin in relation to histone H4K20 methylation levels during the G1 phase using multicolor immunofluorescence-based, single-cell plot analysis (hereafter, referred to as single-cell plot analysis) (27), which is capable of quantitative analysis based on fluorescence microscopic images.

Materials and Methods

Cell culture

hTERT-RPE1 (ATCC, CRL-4000), HeLa (RCB0007), U2OS (ATCC, HTB-96), MRC5 (ATCC, CCL-171), and IMR90 (ATCC, CCL-186) cell lines were grown in a culture medium comprised of high glucose Dulbecco's modified Eagle's medium (Sigma-Aldrich) supplemented with penicillin/streptomycin (100 units/mL penicillin, 100 μg/mL streptomycin; WAKO, Fujifilm) and 10% fetal calf serum (Thermo Fisher Scientific) as described previously (28-30). Contact inhibition was achieved by incubating the confluent cells for four additional days after they covered almost the entire area of the adhesive surface, the medium being changed every day. siRNA transfection was performed using Lipofectamine RNAiMAX (Thermo Fisher Scientific) with siRNAs (SASI_Hs01_00180215 for Set8, SASI_Hs02_00348728 for Suv420h1, and Universal Negative Control #1, Sigma-Aldrich) according to the manufacturer's protocol. Unless otherwise specified, the cells were harvested two days after transfection (> 40 h).

To arrest cell cycle progression at the G1 phase, the cells were treated with 1 μM palbociclib (Sigma-Aldrich) for 18 h.

Immunofluorescence and microscopy

Immunostaining was performed as previously described (29,31) with minor modifications. Cells were plated in a 12-well plate containing a coverslip (15 mm diameter; No. 1S; Matsunami) for more than a day. In the pre-extraction method, cells were immersed in 0.2% Triton X-100 in 20 mM HEPES (pH 7.4) containing 100 mM NaCl and 300 mM sucrose for 5 min on ice and then fixed with 2% paraformaldehyde

(Electron Microscopy Sciences) in 250 mM HEPES (pH 7.4) for 10 min at room temperature (~25 °C). In the direct fixation method, cultured cells were fixed directly without the extraction step. After fixation, cells were permeabilized with 1% Triton X-100 in PBS and blocked with Blocking One (Nacalai Tesque), as described previously (31). The cells were then incubated with the indicated primary antibodies (0.2-1 μg/mL) for 2 h at room temperature (~25 °C), and washed three times with PBS over 30 min. The cells were treated with secondary antibodies (1 μg/mL) and 0.1 μg/mL Hoechst 33342 for 2 h at room temperature (~25 °C) and washed with PBS again. Coverslips were washed with PBS and mounted in Prolong Gold or Prolong Glass antifade (Thermo Fisher Scientific).

The following primary antibodies were used: anti-Mcm3 (sc-390480, mouse, Santa Cruz Biotechnology, 1:1,000 dilution), anti-Mcm2 (D7G11, rabbit, Cell Signaling Technology, 1:1,000 dilution), anti-Mcm2 S108 phosphorylation (EPR4121, rabbit, Abcam,1:400 dilution), anti-Cdt1 (D10F11, rabbit, Cell Signaling Technology, 1:100 dilution), anti-Cdc45 (D7G6, rabbit, Cell Signaling Technology, 1:50 dilution), and anti-Rb phosphorylation (Ser807/811) (D20B12, rabbit, Cell Signaling Technology, 1:400 dilution). For secondary antibodies, the following were purchased: donkey anti-mouse IgG (711-005-151, Jackson ImmunoResearch), donkey anti-rabbit IgG (711-005-152, Jackson ImmunoResearch). The antibodies against histone H4K20me1 (CMA421), H4K20me2 (CMA422) and H4K20me3 (CMA423) were used as described previously (30,32). The direct fixation method was used for immunostaining for Rb phosphorylation.

To label replication foci, cells were incubated in 10 μM EdU for 30 min before fixation, and the signal was detected with Alexa Fluor 647 azide using a Click-iT EdU

Imaging Kit (Thermo Fisher Scientific)(30). For the pulse-label experiments, cells were incubated with 10 μM EdU for 30 min, washed three times with the culture medium, and then cultured until fixation at the indicated times.

Fluorescence images were collected using a DeltaVision Elite system (GE Healthcare Inc.) equipped with a pco.edge 4.2 sCMOS (PCO) and an Olympus 40× UApo/340 oil immersion objective lens (NA 0.65 with iris), with DeltaVision Elite Filter Sets (DAPI-FITC-TRITC-Cy5).

Single-cell plot analysis

Multicolor immunofluorescence-based, single-cell plot analysis was performed as previously described (27). Briefly, the fluorescence intensity of nuclei was measured using the NIS Elements ver 3.0 software (Nikon). The background intensity outside the cells was subtracted from that of the total image, and the nuclear areas of individual cells were determined with automatic thresholding using Hoechst signals. The sum intensity (i.e., the average intensity × nuclear area) in each nucleus was measured for all fluorescence channels. Cells in the M phase were not used for the analysis because the area of condensed chromosomes differed substantially from that of nuclei in the interphase (27). To plot the Hoechst intensity distribution of 400–450 nuclei, the signal intensity in each nucleus was normalized to the nuclei with the 10th lowest and 10th highest intensity, set as 1 and 2, respectively, because the nuclei with the lowest and highest intensity were sometimes outliers. The Hoechst intensity was plotted on a linear scale. The average intensity of EdU, Mcm2/3, Mcm2ph, Rb-ph, histone H4K20me1/me2/me3, Cdt1, and Cdc45 levels was set to 1 (0 on the $\log_2$ scale) and plotted on the $\log_2$ scale. For comparison, the normalized intensity of siRNA the control

was applied to calculate the relative intensities of both the confluent cells and siRNA-treated cells. The values relative to the average were plotted using Mathematica ver. 11 or 12 (Wolfram Research).

Estimation of duration of each cell cycle phase

The total cell cycle length was determined from the growth curves for each cell type (calculated in Fig. 3B). The number of cells in each cell cycle phase was counted based on single-cell plot analysis, except for the M phase; the number of M phase cells was counted based on Hoechst staining in the same preparations. The ratio of the number of cells in each cell cycle phase to the total number of cells was determined, and the duration of each phase was calculated in proportion to the total cell cycle length. Thresholds for selecting cells in each cell cycle phase were as follows: G1 (Hoechst < 1.125 and $\log_2$(EdU) < -3), S ($\log_2$(EdU) > -3), and G2 (Hoechst > 1.7 and $\log_2$(EdU) < -3) phases. The G1 phase was further subdivided into “low MCM” and “high MCM” based on the MCM intensity of cells newly entering the G1 phase at 8 h for each cell type. The values of $\log_2$(Mcm3) thresholding “low MCM” and “high MCM” levels were defined by EdU pulse-labeled experiments as follows: 0.5 for hTERT-RPE1 (Fig. 2A), 0.3 for HeLa, 0.7 for U2OS, 1.0 for MRC5, and 1.5 for IMR90 (Fig. 3A).

ChIP assay

ChIP assays were performed as previously described (31,33) with minor modifications. hTERT-RPE1 cells (7.5×10^6 cells) were first immersed in ice-cold 0.2% Triton X-100 in 20 mM HEPES (pH 7.4) containing 100 mM NaCl and 300 mM sucrose for 5 min, and then cross-linked with a 1% formaldehyde solution (Electron Microscopy Sciences,

Hatfield, PA, USA) for 10 min at room temperature (~25 °C), followed by the quenching step as previously described (31,33). Dynabeads M-280 sheep anti-mouse IgG (30 µL original suspension; Thermo Fisher Scientific) and anti-Mcm3 (2 µg/tube, M038-3, MBL) were used for the immunoprecipitation.

ChIP-seq data analysis

The ChIP-seq library of Mcm3 was prepared using the ThruPLEX DNA-seq Kit (Takara Bio), and sequencing was performed using HiSeq1500 (Illumina). The sequenced reads were aligned to the human genome (hg38) using Bowtie software (version 0.12.8; parameter -v3 -m1). To generate input-normalized ChIP-seq signal tracks (bigWig), deepTools software (34) was used (version 3.3.1; bamCompare parameters: --effectiveGenomeSize 2805636331 --normalizeUsing RPKM --scaleFactorsMethod None -bs 500 --smoothLength 50000). For Orc2, different parameters (bamCoverage: --effectiveGenomeSize 2701495761 --normalizeUsing RPKM -bs 500 --smoothLength 50000) were used due to a lack of input. The statistics and quality check of ChIP-seq data are summarized in Table S1.

Chromatin fractionation and sucrose gradient centrifugation

Fractions of native chromatin were prepared as previously described (35-37) with some modifications to human cells. hTERT-RPE1 cells (1×10^7 cells) were washed with cold PBS, and the subsequent steps were performed on ice. The cells were collected with buffer A (50 mM HEPES (pH 7.4), 100 mM KCl, 2.5 mM $MgCl_2$, 0.1 mM $ZnSO_4$, 1 mM ATP, 1 mM DTT, PhosSTOP^{TM} tablets (Roche), and protease inhibitor cocktail (EDTA-free, Nacalai Tesque, Inc.)). The cells were transferred into 1.5-mL tubes,

centrifuged (1300 × *g*, 3 min, 4 °C), and resuspended in buffer A containing 0.2% Triton X-100. The aliquots were fractionated using a sucrose gradient in 400 µL of buffer A containing 0.2% Triton X-100 and 30% sucrose, and centrifuged (20,000 × *g*, 10 min, 4 °C). The supernatant (Sup) contained non-chromatin-bound proteins, while the chromatin-bound proteins were in the Pellet (Fig. 5A). The Pellet was washed with buffer A containing 0.2% Triton X-100, resuspended in buffer B (50 mM HEPES (pH 7.4), 10 mM KCl, 2 mM $MgCl_2$, 0.1 mM $ZnSO_4$, 3 mM ATP, 1 mM DTT, PhosSTOP™ tablets (Roche), protease inhibitor cocktail (EDTA-free, Nacalai Tesque)) supplemented with 200 U/mL of benzonase (Millipore) for 1 h at 4 °C. The samples were then centrifuged at 40,000 rpm (~128,000 × *g*) for 3 h at 4 °C using an MLS-5 rotor (Beckman Coulter). After centrifugation, the fractions (350 µL each) were collected from the top of the gradient and subjected to SDS-PAGE analysis and immunoblotting. Aldolase (158 kDa) and thyroglobulin (669 kDa) were used as protein size markers. After acetone precipitation, methanol/chloroform protein precipitation was performed to remove the sucrose. The precipitate was dissolved in 40 µL of 2 × SDS loading buffer at room temperature (~25 °C) overnight.

A 5 µL sample was used for Western blot analysis with the anti-Mcm2 antibody (D7G11, rabbit, Cell Signaling Technology, 1:1000 dilution) or the anti-Cdc45 antibody (D7G6, rabbit, Cell Signaling Technology, 1:1000 dilution).

Results

Cell-cycle dynamics of MCM revealed by single-cell plot analysis

To investigate the loading of the MCM complex onto chromatin during the G1 phase in human cells, we used hTERT-immortalized retinal pigment epithelial (hTERT-RPE1) cells. hTERT-RPE1 cells can be arrested in the G1 phase, unlike cancerous cells (38,39). An asynchronous cell population was simultaneously labeled with Hoechst 33342 (DNA amount indicator), EdU (S phase indicator), and Mcm3 (Fig. 1A). The total amount of Mcm3 was detected by directly fixing the cells, and the chromatin-bound fraction of Mcm3 was detected in cells fixed after the pre-extraction step using a nonionic detergent (40,41) (in this method, the chromatin-bound fraction does not distinguish between associated and stably-loaded MCM hexamers). The normalized intensities of EdU and Mcm3 in the same cell were plotted against the DNA content estimated from Hoechst intensity (Fig. 1B). Cells displaying EdU intensity > 0.125 (-3.0 on the $\log_2$ scale), plotted as orange dots in the EdU panels, represent cells undergoing DNA replication in the S phase, and the same cells were also plotted as orange dots in the Mcm3 panels. In the direct fixation method, Mcm3 intensities showed relatively small variations ranging from 0.50 to 1.68 (-1.0 to 0.75 on the $\log_2$ scale) throughout the cell cycle. In contrast, in the pre-extraction method, the intensities of chromatin-bound Mcm3 displayed large variations, as shown previously (39,42,43), ranging from 0.25 to 2.83 (-2.0 to 1.5 on the $\log_2$ scale) during the G1 phase (Fig. 1B). Mcm3 levels were highest at the G1/S transition, decreased during the S phase, and reached the lowest levels in the G2 phase. In this study, we used the pre-extraction method to detect the chromatin-bound fraction of MCM complex, which include associated and stably-loaded MCM hexamers. We confirmed that both Mcm2 and Mcm3 proteins reproduced

similar results in intracellular localization (Fig. S1A) and patterns of the single-cell plot analysis (Fig. S1B). These results were also consistent with the behavior of Mcm4 in living cells as reported previously (44). Thus, we used Mcm2 and Mcm3 proteins to represent the dynamics of the MCM complex.

To examine how Mcm3 intensities change during the cell cycle, cells were pulse-labeled with EdU for 30 min and then cultured without EdU for up to 24 h. The normalized intensities of EdU and Mcm3 in the same cell were plotted against the Hoechst intensity (Fig. 2A). Cells undergoing S phase when pulse-labeled with EdU at 0 h (EdU > 0.125; -3.0 on the $\log_2$ scale) were plotted as orange dots (see Fig. 2A upper leftmost panel, 0 h). The orange dots in the EdU panels (representing S phase cells at 0 h) were plotted at different positions against the Hoechst intensity over time after the pulse label (4–24 h in Fig. 2A upper panels). Four to eight hours after the pulse label, most of the orange-marked cells proceeded from the mid/late S phase to G2 phase as indicated by an increase in the Hoechst intensity. After 8–12 h, a part of the orange-marked cell population proceeded through the M phase and entered the G1 phase as indicated by low Hoechst intensity, and after 16 h, some cells entered the S phase again. After 20–24 h, most orange-marked cells again displayed a middle range of Hoechst intensities with a pattern similar to that of cells at 0 h, consistent with the doubling time in this cell line (approximately 22.5 h; see Fig. 3B below). Using the EdU pattern as a cell cycle landmark, we analyzed cell-cycle changes of Mcm3 (Fig. 2A, lower panels). The S phase cells at 0 h were also plotted as orange dots in the Mcm3 panels. Mcm3 levels were highest (> 2; 1 on the $\log_2$ scale) in the early S phase (Hoechst intensity around 1.2; 0 h), and decreased during the late S phase (4 h). After 8 h, the orange-marked G1 cells showed low to moderate Mcm3 intensity levels (< 1.44; 0.5 on the $\log_2$

scale; termed as “low MCM” fraction), whereas higher Mcm3 intensity levels appeared after 12 h (> 1.44; 0.5 on the $\log_2$ scale; termed as “high MCM” fraction). The increase in Mcm3 levels from the “low MCM” fraction to the “high MCM” fraction suggested that more MCM complexes bound to chromatin in the late G1 phase.

Next, using a pre-extraction method, we investigated the profile of Cdt1 protein (Fig. 2B, 2C, Fig. S2A), which promotes the loading of MCM complexes onto chromatin (18). Single-cell plot analysis of Cdt1 and EdU revealed that the Cdt1 intensities showed large variations in G1 cells (Hoechst < 1.125), and remained low after the S phase (Fig. S2A), consistent with previous reports (45,46). Single-cell plot analysis of Cdt1 and Mcm3 revealed that the cells with higher Cdt1 levels (> 2.82; 1.5 on the $\log_2$ scale; displayed as pink dots in Fig. 2C left panel) showed relatively higher levels of Mcm3 (> 1.44; 0.5 on the $\log_2$ scale; pink dots in Fig. 2C right panel). The state of pink dots is a transient event because cells that showed higher levels of Cdt1 occupied approximately 4.6% ± 2.3% (n = 5) of the cell population. This result suggested that large amounts of Cdt1 protein were temporarily required for the loading of high levels of MCM to chromatin. We confirmed that the cells with “high MCM” also showed high phosphorylation levels of Mcm2 (S108ph; Fig. S2B, S2C), which occurred before and during the S phase (47,48).

MCM loading dynamics during the cell cycle were also examined by EdU pulse-label experiments in other cell types including cancer (HeLa and U2OS) and normal (MRC5 and IMR90) cell lines (Fig. 3A). MCM levels in these cells showed dynamics similar to those in hTERT-RPE1 cells. The orange-marked G1 cells showed low to moderate Mcm3 intensity levels 8 h after EdU pulse-labeling. Then the MCM levels decreased in the S phase, and reached the lowest levels in the G2 phase (Fig. 3A).

The cells with "low MCM" were more abundant in MRC5 and IMR90 cells than in hTERT-RPE1, HeLa, and U2OS cells. As MRC5 and IMR90 cells showed longer doubling times (Fig. 3B), we examined which cell cycle stages were prolonged in these cells (Fig. 3C). The duration of each cell cycle stage was estimated using single-cell plot analysis based on Hoechst, MCM, and EdU levels (8 h in Fig. 3A). Although the duration of "high MCM" was 2–4 h in all the cell lines examined, the duration of the "low MCM" G1 phase was 20–27 h in MRC5 and IMR90 cells and 8–9 h in hTERT-RPE1, HeLa, and U2OS cells (Fig. 3C). Therefore, the prolonged doubling time was attributed to the high proportion of "low MCM" in the G1 phase. These results indicate that cells just entering the G1 phase spent several hours with "low MCM", followed by 2–4 h of "high MCM" in the late G1 phase.

The normal cells that remained in the G1 phase for a long time (G1 gray cells at 8 h in Fig 3A, MRC5 and IMR90) showed relatively lower levels of Mcm3 (< 0.25; -2 on the $\log_2$ scale), similar to those in the G2 phase. This result raised a question of whether the normal cells remaining for a long time in the G1 phase may represent a different proliferating state. We examined phosphorylation levels of retinoblastoma protein (Rb), which is necessary for cell cycle progression during the G1 phase (49-51) (Fig. S3). Levels of Rb phosphorylation at Ser807/811 were lower in the majority of MRC5 cells at the G1 phase (square regions in Fig. S3) than those in newly entering G1 cells (G1 orange cells in Fig. S3). Such low levels of Rb phosphorylation were rarely observed in proliferating hTERT-RPE1 cells (square regions in Fig. S3). These results suggest that MRC5 cells at the G1 phase have an additional pausing phase during the cell cycle progression.

MCM dynamics under the G1 arrest conditions

To investigate the state of MCM loading in G1 arrest cells, the cell cycle progression was halted under two conditions in hTERT-RPE1 cells (Fig. 4A, 4B). One condition was via contact inhibition by culturing the cells to confluence. The other condition was using siRNA treatment for more than 40 h to target the gene encoding Set8, the methyltransferase for histone H4K20 monomethylation (H4K20me1)(52,53). In both cases, the number of EdU-positive cells was low and most of the cells showed low Hoechst intensity (Fig. 4B), suggesting that these cells were arrested in the G1 phase. Remarkably, the cells treated with Set8-siRNA showed a complete decrease in the levels of histone H4K20me1 (< -3; 0.125 on the $\log_2$ scale), whereas the confluent cells showed low to moderate levels of histone H4K20me1 from -3 to 0 (0.125 to 1 on the $\log_2$ scale). In this regard, the Set8-siRNA-treated cells showed high MCM levels (> 0.70; -0.5 on the $\log_2$ scale) that were sufficient for entry into the S phase, as shown previously (26,54) whereas the Mcm2 intensity was low to moderate, from 0.05 to 0.71 (-4.5 to -0.5 on the $\log_2$ scale) in the confluent cells. These results indicate that confluent hTERT-RPE1 cells were arrested at a “low MCM” level similar to the normal cell lines (MRC5 and IMR90) in Fig. 3A, and Set8-siRNA-treated cells were arrested at a “high MCM” level in the G1 phase.

Genome-wide distribution of MCM3 proteins

To examine the differences in MCM binding preferences in the genome during early or late G1 phases (corresponding to the “low” and “high” MCM state, respectively), we first determined the genomic distribution of MCM binding with chromatin immunoprecipitation followed by DNA sequencing (ChIP-seq) analysis with the Mcm3

antibody. The asynchronous population of cells in the growth phase was pre-extracted before fixation, followed by normal preparation for ChIP-seq experiments (31,33). Using this method with the Mcm3 antibody, chromatin prepared from 7.5×10^6 cells produced significant enrichment of the Mcm3 peaks (Fig. 4C, Table S1), which was similar to the Mcm7 peaks (55). Then, the Mcm3 profile was compared with the previous reports on Orc2 ChIP-seq data (56) and SNS-seq data (sequences of short, nascent DNA single strands reflecting replication initiation)(57). Orc2 is required for the loading of MCM protein complexes, and is regarded as a marker of replication origin (17). The pattern of Mcm3 peaks was similar to the Orc2 and SNS peaks, indicating that the MCM complex accumulated at the replication origin (Fig. 4C, Fig. S4A). However, in some chromosomes that show late replication initiation (58), the SNS and MCM proteins were less accumulated, whereas the Orc2 peaks were detectable, for example, in chromosome 6 (Fig. S4B). Because Orc2 remains on the chromatin throughout the cell cycle (59,60), these results suggest that MCM abundance is a mark of early replication rather than the Orc2-marked replication origin.

Next, to determine whether the variations in Mcm3 intensity of immunostaining during the G1 phase as observed in Fig. 4B reflects the changes in its localization along the chromosome, we examined Mcm3 distribution in growth phase cells and G1-arrested cells (confluent cells and Set8-siRNA-treated cells) using ChIP-seq experiments. The genome-wide localization patterns of Mcm3 were almost indistinguishable among those cells (Fig. 4C, Table S1), indicating that variations shown in immunostaining do not influence the genomic localization pattern of MCM.

Single and double MCM hexamers in G1 arrest cells

The increased amount of MCM revealed by the immunostaining experiment may reflect the conversion of a single to double hexamer of the MCM complex, as reported previously (15,16,61). To consider this possibility, we next examined the sizes of the MCM complex using a sucrose gradient ultracentrifugation method (7,36,37) with some modifications (Fig. 5A, see Methods). Lysates of the asynchronous population of growing cells were separated into a chromatin-unbound fraction (Sup) and a chromatin-bound fraction (Pellet). After performing sucrose density gradient ultracentrifugation, each fraction was collected and subjected to Western blot analysis (Fig. 5B). A band at a position below the molecular marker of 150 kDa was detected using the Mcm2 antibody, reflecting the molecular mass of a single Mcm2 protein without modification (100.9 kDa). Mcm2 was detected in fractions 1–10 in the Sup fraction and was especially high in fractions 1–3. Fractions 1–2 corresponded to free Mcm2 protein, and fraction 2–3 corresponded to a single MCM hexamer, as a single MCM hexamer without a modification was estimated to be ~545 kDa. In the Pellet, Mcm2 was detected in fraction 6 in addition to fractions 3 and 4. It is likely that the larger peak (fraction 6) corresponded to a double MCM hexamer, as shown previously in yeast (37). In the confluent cells, the majority of MCM in the Pellet was found in the fractions 3–4 with some extension to larger fractions (up to fraction 7). Most of the Mcm2 proteins in the cells treated with Set8-siRNA were incorporated into the Pellet and were scarcely present in the Sup fraction. In the Pellet from these cells, the Mcm2 proteins were abundantly present in fractions 5–6, which corresponded to a double MCM hexamer. These results suggest that the single and double MCM hexamers detected in size fractionation corresponded to the low and high levels of MCM in immunostaining, respectively.

We further confirmed the states of the MCM complex by using G1 cells arrested with palbociclib. Palbociclib is an inhibitor of Cdk4/6 activity, which is required for cell cycle progression from G1 to S phase (62,63). Single-cell plot analysis with MCM antibody showed that treatment with palbociclib enriched the low MCM state at the G1 phase (Fig. 5C). Sucrose gradient experiment followed by Western blot analysis revealed that the MCM proteins in the palbociclib-treated cells were detected in fractions 2–4 (Fig. 5D). In contrast, the signal in fraction 6, as seen in growth phase cells, was not detected in the palbociclib-treated cells, indicating the absence of a double MCM hexamer. These results confirmed that the "low MCM" state in the palbociclib-treated cells was composed of single hexamers.

We then examined the presence of the Cdc45 protein, which binds to the MCM complex and functions as a DNA helicase (64-66). In growth phase cells, single-cell plot analysis revealed that most of Cdc45 positive cells (> 1; 0 on the $\log_2$ scale) were in the S phase and some of them were in the "high MCM" state of the G1 phase (Fig. 5E). In Western blot analysis using the same samples in Fig. 5D, Cdc45 was abundant in fractions 3–7 in growth phase cells (Fig. 5F), indicating that Cdc45 was contained in both "low MCM" and "high MCM" states corresponding to the single and double MCM hexamer, respectively, in growth phase cells. In contrast, Cdc45 was not detected in cells treated with palbociclib (Fig. 5F). Thus, we concluded that the palbociclib-treated cells were arrested in the early G1 phase before loading Cdc45. We also examined the Cdc45 protein in chromatin-bound fractions in confluent cells and SET8-siRNA-treated cells to understand their cell cycle stages. Cdc45 was absent in confluent cells and present in SET8-siRNA-treated cells (Fig. S5A, B), suggesting that

the cell cycle in confluent cells and SET8-siRNA-treated cells was arrested at the early and late G1 phases, respectively.

The single-cell plot and sucrose gradient fractionation analyses detected MCM double hexamers in cells treated with Set8-siRNA for more than 40 h. This raised the question of whether MCM could be loaded onto chromatin as a double hexamer in early G1 cells depleted of Set8. To address this question, we examined the MCM hexamer states in early G1 cells depleted of Set8 (Fig. 6). SET8-siRNA treatment followed by an EdU pulse-label experiment was performed to detect MCM levels. The levels of H4K20me1 decreased in cells treated with Set8-siRNA for 18 h, indicating that the duration of siRNA treatment was effective in depleting Set8 protein levels. Four hours after EdU removal, the orange dots (EdU > 0.125; -3.0 on the log2 scale) migrated from S to G2 phase in the control cells, whereas some orange dots remained in the S phase in siRNA-treated cells, suggesting that the cell cycle of these cells was arrested. To highlight the cells just entering G1 in the 8 h panel, only dots with high levels of EdU were colored blue (Hoechst < 1.125, EdU > 1; 0 on the log2 scale; the squares in the EdU panels in Fig. 6). In these blue-marked Set8-siRNA-treated cells, the Mcm2 levels remained within a range from 0.5 to 1.44 (-1 to 0.5, on the $\log_2$ scale; blue dots in the Mcm2 panels in Fig. 6), suggesting a single hexamer state of the MCM complex. These results indicate that MCM complexes in siRNA-treated cells are loaded onto chromatin as a single hexamer in the early G1 phase. Double MCM hexamers found after longer treatment with Set8-siRNA (Fig. 4B, Fig. 5B) were probably formed by the residual amount of H4K20me2/3 in these cells. Indeed, the levels of H4K20me2/3 in Set8-siRNA cells were similar to those in control cells (Fig.7D).

MCM hexamer states and levels of histone H4K20 methylation

To examine the relationship between the levels of MCM and histone H4K20 methylation in hTERT-RPE1 cells, asynchronized cells were co-immunostained with antibodies against Mcm2, H4K20me1, and H4K20me2/me3 (Fig. 7A, Fig.S6A). The level of histone H4K20me1 increased during the G2 phase and remained high in the M phase, and cells immediately after division also showed relatively high H4K20me1 intensity (Fig. 7B, left), as shown previously (27,30,67). G1-phase cells with high levels of histone H4K20me1 (> 1.23; 0.3 on the $\log_2$ scale) were selected and plotted as light blue dots (Fig. 7B upper). The same cells were also plotted as light blue dots in the H4K20me2 and Mcm2 panels (Fig. 7B upper), showing relatively low levels of H4K20me2 and Mcm2 among the G1 cells. In the middle panel of Fig. 7B, cells with low H4K20me2 levels (< 1.07; -0.1 on the $\log_2$ scale) were selected and plotted as blue dots; these cells showed high H4K20me1 levels and low Mcm2 levels. When G1 cells with high Mcm2 levels (> 1.44; 0.5 on the log2 scale; pink dots in Fig. 7B bottom) were selected, these cells showed low H4K20me1 levels and high H4K20me2. A scatter plot of these dots against H4K20me1 and Mcm2 intensities indicated that the light blue (high H4K20me1 levels) and pink (high MCM levels) dots were mutually exclusive (Fig. 7C upper). In addition, the blue (low H4K20me2 levels) and pink (high Mcm2 levels) dots were mutually exclusive (Fig. 7C bottom); similar results were also obtained for H4K20me3 (Fig.S6B, S6C), indicating that the decrease in H4K20me1 levels reflects an increase in H4K20me2/me3. These results suggest that MCM proteins likely form a single hexamer on the chromatin when the H4K20me1 levels are high, and the MCM complex forms a double hexamer after H4K20me1 is converted to H4K20me2/me3 during G1-phase progression.

To confirm that the conversion of H4K20me1 to H4K20me2/me3 is necessary for the transition from the single to the double state of MCM hexamers, cells were treated with siRNA of Suv420h1, the enzyme responsible for this conversion. Compared with control cells, the Suv420h1-siRNA-treated cells showed lower H4K20me2/me3 levels and a "low MCM" state (Fig.7D). These results suggest that the conversion of H4K20me1 to H4K20me2/me3 is essential for pre-RC formation.

Discussion

This study demonstrated that MCM complexes on chromatin convert from a single hexamer to a double hexamer in association with di-/tri-methylation of histone H4K20 toward S phase entry. Our results, in combination with previous reports (reviewed in 68), propose the following model (Fig 8). MCM complexes are initially loaded onto chromatin as a single hexamer after entry into the G1 phase. The MCM complex forms a single hexamer without Cdc45 in the early G1 phase (state 1). This state can also be seen in the cells arrested by treatment with palbociclib or by contact inhibition in the confluent cells. These complexes are subsequently transformed into double hexamers before entering the S phase (state 2). Then, Cdc45 is loaded onto the MCM double hexamer to initiate DNA replication in the S phase (state 3). As Set8 is required for S-phase progression (69), Set8-depleted cells are arrested around the G1/S transition. Once DNA replication is initiated, the MCM double hexamer containing Cdc45 converts to the MCM single hexamer containing Cdc45 (state 4) as the replication forks progress as in growth phase cells. The transition of the single to double hexamer of MCM is triggered by the conversion of H4K20me1 to H4K20me2/me3.

Normal cells (MRC5 and IMR90) or hTERT-RPE1 cells arrested via contact inhibition showed that cell populations in the single MCM hexamer state increased, compared with HeLa and U2OS cancer cells, indicating that normal cells pause at the single MCM hexamer state longer than cancer cells during the G1 phase. In comparison, the duration of the double hexamer state in the cell cycle was unchanged across cell types. These results suggest that MCM loading onto chromatin pauses at the single hexamer state in the G1 phase and can stay halted there if conditions favor a non-proliferating state. In contrast, once the double hexamer forms, the cell cycle proceeds to enter the S phase for cell proliferation. Therefore, halting at the single MCM hexamer state is a limiting step for the decision of cell proliferation or quiescence. The transition from the single to double hexamer state of MCM can be affected by the activation of several factors associated in exiting the G1 arrest (2,10,70). In fact, when the cells were treated with palbociclib, the MCM complex remained in the single hexamer state without conversion to the double hexamer. Palbociclib treatment inhibits the activity of Cdk4/6 leading to inactivation of the Rb protein, suggesting that the conversion of the MCM state from a single to double hexamer is regulated by G1 progression. Rb is mutated or functionally inactivated in the majority of cancer cells (71,72), supporting our results showing that cancer cells pass through the single-to-double MCM hexamer conversion more quickly than normal cells.

Histone modifications, especially methylation at histone H4K20, may be one of the important factors for regulating the loading of the second MCM complex. Our results indicate that the levels of histone di-/tri-methylation at H4K20 correlatively increased prior to the loading of the second MCM hexamer (Fig. 7; Fig. S6), suggesting that the conversion of H4K20me1 to H4K20me2/me3 is required for loading of the

second MCM hexamers. As our results suggest that the timing of loading of the second MCM hexamer ("high MCM" state) determines the timing of G1 progression to the S phase (Fig. 3C), the conversion of H4K20me1 to H4K20me2/me3 seems to be an important factor in determining S phase progression. Although the factors that cause the transition of the histone modification state remain unknown, our findings revealed the relationship between the process of pre-RC formation and histone modifications during the G1 phase, and therefore will provide new insights into the mechanism of the proliferation-quiescence decision.

Data availability

ChIP-seq data were submitted to Gene Expression Omnibus (GEO) with the accession number: GSE157839. Further data are available from the corresponding authors upon reasonable request.

Funding

This work was supported by JSPS KAKENHI grants: JP25116006, JP17H03636 and JP18H05528 (to TH); JP18H05527 (to YO and HK); JP18H04802, JP19H05244, JP17H03608, JP20H00456, JP20H04846 and JP20K21398 (to YO); JP18H05532, JP18H04713 and JP19H03156 (to CO); JP18H05533 and JP20H00454 (to Y Hiraoka). This work was also supported by the Naito Foundation and the Urakami Foundation (to YHT). This work was partly performed in the cooperative research project program of the medical institute of bioregulation, Kyushu University.

Conflict of interest

The authors declare no competing interests.

Acknowledgements

We also thank Drs. Keiichi Namba and Tomoko Miyata (Osaka University) for their kind supports in protein biochemistry experiments.

References

1. Massagué, J. (2004) G1 cell-cycle control and cancer. *Nature*, **432**, 298-306.
2. Pack, L.R., Daigh, L.H. and Meyer, T. (2019) Putting the brakes on the cell cycle: mechanisms of cellular growth arrest. *Curr Opin Cell Biol*, **60**, 106-113.
3. Matson, J.P. and Cook, J.G. (2017) Cell cycle proliferation decisions: the impact of single cell analyses. *Febs j*, **284**, 362-375.
4. Hume, S., Dianov, G.L. and Ramadan, K. (2020) A unified model for the G1/S cell cycle transition. *Nucleic Acids Res*, **48**, 12483-12501.
5. Zetterberg, A., Larsson, O. and Wiman, K.G. (1995) What is the restriction point? *Curr Opin Cell Biol*, **7**, 835-842.
6. Remus, D., Beuron, F., Tolun, G., Griffith, J.D., Morris, E.P. and Diffley, J.F. (2009) Concerted loading of Mcm2-7 double hexamers around DNA during DNA replication origin licensing. *Cell*, **139**, 719-730.
7. Evrin, C., Clarke, P., Zech, J., Lurz, R., Sun, J., Uhle, S., Li, H., Stillman, B. and Speck, C. (2009) A double-hexameric MCM2-7 complex is loaded onto origin DNA during licensing of eukaryotic DNA replication. *Proc Natl Acad Sci U S A*, **106**, 20240-20245.
8. Bell, S.D. and Botchan, M.R. (2013) The minichromosome maintenance replicative helicase. *Cold Spring Harb Perspect Biol*, **5**, a012807.
9. Deegan, T.D. and Diffley, J.F. (2016) MCM: one ring to rule them all. *Curr Opin Struct Biol*, **37**, 145-151.
10. Limas, J.C. and Cook, J.G. (2019) Preparation for DNA replication: the key to a successful S phase. *FEBS Lett*, **593**, 2853-2867.
11. Hoshina, S., Yura, K., Teranishi, H., Kiyasu, N., Tominaga, A., Kadoma, H., Nakatsuka, A., Kunichika, T., Obuse, C. and Waga, S. (2013) Human origin recognition complex binds preferentially to G-quadruplex-preferable RNA and single-stranded DNA. *J Biol Chem*, **288**, 30161-30171.
12. Langley, A.R., Gräf, S., Smith, J.C. and Krude, T. (2016) Genome-wide identification and characterisation of human DNA replication origins by initiation site sequencing (ini-seq). *Nucleic Acids Res*, **44**, 10230-10247.
13. Stinchcomb, D.T., Thomas, M., Kelly, J., Selker, E. and Davis, R.W. (1980) Eukaryotic DNA segments capable of autonomous replication in yeast. *Proc Natl Acad Sci U S A*, **77**, 4559-4563.
14. Liachko, I., Youngblood, R.A., Keich, U. and Dunham, M.J. (2013) High-resolution mapping, characterization, and optimization of autonomously replicating sequences in yeast. *Genome Res*, **23**, 698-704.
15. Fernandez-Cid, A., Riera, A., Tognetti, S., Herrera, M.C., Samel, S., Evrin, C., Winkler,

C., Gardenal, E., Uhle, S. and Speck, C. (2013) An ORC/Cdc6/MCM2-7 complex is formed in a multistep reaction to serve as a platform for MCM double-hexamer assembly. *Mol Cell*, **50**, 577-588.

16. Ticau, S., Friedman, L.J., Ivica, N.A., Gelles, J. and Bell, S.P. (2015) Single-molecule studies of origin licensing reveal mechanisms ensuring bidirectional helicase loading. *Cell*, **161**, 513-525.
17. Takeda, D.Y., Shibata, Y., Parvin, J.D. and Dutta, A. (2005) Recruitment of ORC or CDC6 to DNA is sufficient to create an artificial origin of replication in mammalian cells. *Genes Dev*, **19**, 2827-2836.
18. Frigola, J., He, J., Kinkelin, K., Pye, V.E., Renault, L., Douglas, M.E., Remus, D., Cherepanov, P., Costa, A. and Diffley, J.F.X. (2017) Cdt1 stabilizes an open MCM ring for helicase loading. *Nat Commun*, **8**, 15720.
19. Miller, T.C.R., Locke, J., Greiwe, J.F., Diffley, J.F.X. and Costa, A. (2019) Mechanism of head-to-head MCM double-hexamer formation revealed by cryo-EM. *Nature*, **575**, 704-710.
20. Yuan, Z., Schneider, S., Dodd, T., Riera, A., Bai, L., Yan, C., Magdalou, I., Ivanov, I., Stillman, B., Li, H. *et al.* (2020) Structural mechanism of helicase loading onto replication origin DNA by ORC-Cdc6. *Proc Natl Acad Sci U S A*, **117**, 17747-17756.
21. Smith, O.K. and Aladjem, M.I. (2014) Chromatin structure and replication origins: determinants of chromosome replication and nuclear organization. *J Mol Biol*, **426**, 3330-3341.
22. Jørgensen, S., Schotta, G. and Sørensen, C.S. (2013) Histone H4 lysine 20 methylation: key player in epigenetic regulation of genomic integrity. *Nucleic Acids Res*, **41**, 2797-2806.
23. Oda, H., Hübner, M.R., Beck, D.B., Vermeulen, M., Hurwitz, J., Spector, D.L. and Reinberg, D. (2010) Regulation of the histone H4 monomethylase PR-Set7 by CRL4(Cdt2)-mediated PCNA-dependent degradation during DNA damage. *Mol Cell*, **40**, 364-376.
24. Brustel, J., Kirstein, N., Izard, F., Grimaud, C., Prorok, P., Cayrou, C., Schotta, G., Abdelsamie, A.F., Déjardin, J., Méchali, M. *et al.* (2017) Histone H4K20 tri-methylation at late-firing origins ensures timely heterochromatin replication. *Embo j*, **36**, 2726-2741.
25. Beck, D.B., Burton, A., Oda, H., Ziegler-Birling, C., Torres-Padilla, M.E. and Reinberg, D. (2012) The role of PR-Set7 in replication licensing depends on Suv4-20h. *Genes Dev*, **26**, 2580-2589.
26. Shoaib, M., Walter, D., Gillespie, P.J., Izard, F., Fahrenkrog, B., Lleres, D., Lerdrup, M.,

Johansen, J.V., Hansen, K., Julien, E. *et al.* (2018) Histone H4K20 methylation mediated chromatin compaction threshold ensures genome integrity by limiting DNA replication licensing. *Nat Commun*, **9**, 3704.

27. Hayashi-Takanaka, Y., Kina, Y., Nakamura, F., Becking, L.E., Nakao, Y., Nagase, T., Nozaki, N. and Kimura, H. (2020) Histone modification dynamics as revealed by multicolor immunofluorescence-based single-cell analysis. *J Cell Sci*, **133**. jcs243444.
28. Tsuchiya, M., Ogawa, H., Suzuki, T., Sugiyama, N., Haraguchi, T. and Hiraoka, Y. (2011) Exportin 4 interacts with Sox9 through the HMG Box and inhibits the DNA binding of Sox9. *PLoS One*, **6**, e25694.
29. Hayashi-Takanaka, Y., Yamagata, K., Wakayama, T., Stasevich, T.J., Kainuma, T., Tsurimoto, T., Tachibana, M., Shinkai, Y., Kurumizaka, H., Nozaki, N. *et al.* (2011) Tracking epigenetic histone modifications in single cells using Fab-based live endogenous modification labeling. *Nucleic Acids Res*, **39**, 6475-6488.
30. Hayashi-Takanaka, Y., Maehara, K., Harada, A., Umehara, T., Yokoyama, S., Obuse, C., Ohkawa, Y., Nozaki, N. and Kimura, H. (2015) Distribution of histone H4 modifications as revealed by a panel of specific monoclonal antibodies. *Chromosome Research*, **23**, 753-766.
31. Kimura, H., Hayashi-Takanaka, Y., Goto, Y., Takizawa, N. and Nozaki, N. (2008) The organization of histone H3 modifications as revealed by a panel of specific monoclonal antibodies. *Cell Struct Funct*, **33**, 61-73.
32. Hayashi-Takanaka, Y., Stasevich, T.J., Kurumizaka, H., Nozaki, N. and Kimura, H. (2014) Evaluation of chemical fluorescent dyes as a protein conjugation partner for live cell imaging. *PLoS One*, **9**, e106271.
33. Kaimori, J.-Y., Maehara, K., Hayashi-Takanaka, Y., Harada, A., Fukuda, M., Yamamoto, S., Ichimaru, N., Umehara, T., Yokoyama, S. and Matsuda, R. (2016) Histone H4 lysine 20 acetylation is associated with gene repression in human cells. *Scientific reports*, **6**, 24318.
34. Ramirez, F., Ryan, D.P., Gruning, B., Bhardwaj, V., Kilpert, F., Richter, A.S., Heyne, S., Dundar, F. and Manke, T. (2016) deepTools2: a next generation web server for deep-sequencing data analysis. *Nucleic Acids Res*, **44**, W160-165.
35. Méndez, J. and Stillman, B. (2000) Chromatin association of human origin recognition complex, cdc6, and minichromosome maintenance proteins during the cell cycle: assembly of prereplication complexes in late mitosis. *Mol Cell Biol*, **20**, 8602-8612.
36. Sheu, Y.J. and Stillman, B. (2006) Cdc7-Dbf4 phosphorylates MCM proteins via a docking site-mediated mechanism to promote S phase progression. *Mol Cell*, **24**, 101-113.

37. Quan, Y., Xia, Y., Liu, L., Cui, J., Li, Z., Cao, Q., Chen, X.S., Campbell, J.L. and Lou, H. (2015) Cell-Cycle-Regulated Interaction between Mcm10 and Double Hexameric Mcm2-7 Is Required for Helicase Splitting and Activation during S Phase. *Cell Rep*, **13**, 2576-2586.
38. Sun, X., Bizhanova, A., Matheson, T.D., Yu, J., Zhu, L.J. and Kaufman, P.D. (2017) Ki-67 Contributes to Normal Cell Cycle Progression and Inactive X Heterochromatin in p21 Checkpoint-Proficient Human Cells. *Mol Cell Biol*, **37**. e00569-16.
39. Matson, J.P., House, A.M., Grant, G.D., Wu, H., Perez, J. and Cook, J.G. (2019) Intrinsic checkpoint deficiency during cell cycle re-entry from quiescence. *J Cell Biol*, **218**, 2169-2184.
40. Jasencakova, Z., Scharf, A.N., Ask, K., Corpet, A., Imhof, A., Almouzni, G. and Groth, A. (2010) Replication stress interferes with histone recycling and predeposition marking of new histones. *Mol Cell*, **37**, 736-743.
41. Aparicio, T., Megias, D. and Mendez, J. (2012) Visualization of the MCM DNA helicase at replication factories before the onset of DNA synthesis. *Chromosoma*, **121**, 499-507.
42. Haland, T.W., Boye, E., Stokke, T., Grallert, B. and Syljuasen, R.G. (2015) Simultaneous measurement of passage through the restriction point and MCM loading in single cells. *Nucleic Acids Res*, **43**, e150.
43. Hiraga, S.I., Ly, T., Garzon, J., Horejsi, Z., Ohkubo, Y.N., Endo, A., Obuse, C., Boulton, S.J., Lamond, A.I. and Donaldson, A.D. (2017) Human RIF1 and protein phosphatase 1 stimulate DNA replication origin licensing but suppress origin activation. *EMBO Rep*, **18**, 403-419.
44. Kuipers, M.A., Stasevich, T.J., Sasaki, T., Wilson, K.A., Hazelwood, K.L., McNally, J.G., Davidson, M.W. and Gilbert, D.M. (2011) Highly stable loading of Mcm proteins onto chromatin in living cells requires replication to unload. *J Cell Biol*, **192**, 29-41.
45. Nishitani, H., Taraviras, S., Lygerou, Z. and Nishimoto, T. (2001) The human licensing factor for DNA replication Cdt1 accumulates in G1 and is destabilized after initiation of S-phase. *J Biol Chem*, **276**, 44905-44911.
46. Rialland, M., Sola, F. and Santocanale, C. (2002) Essential role of human CDT1 in DNA replication and chromatin licensing. *J Cell Sci*, **115**, 1435-1440.
47. Montagnoli, A., Valsasina, B., Brotherton, D., Troiani, S., Rainoldi, S., Tenca, P., Molinari, A. and Santocanale, C. (2006) Identification of Mcm2 phosphorylation sites by S-phase-regulating kinases. *J Biol Chem*, **281**, 10281-10290.
48. Chuang, L.C., Teixeira, L.K., Wohlschlegel, J.A., Henze, M., Yates, J.R., Mendez, J. and Reed, S.I. (2009) Phosphorylation of Mcm2 by Cdc7 promotes pre-replication

complex assembly during cell-cycle re-entry. *Mol Cell*, **35**, 206-216.

49. Murphree, A.L. and Benedict, W.F. (1984) Retinoblastoma: clues to human oncogenesis. *Science*, **223**, 1028-1033.
50. Rubin, S.M. (2013) Deciphering the retinoblastoma protein phosphorylation code. *Trends Biochem Sci*, **38**, 12-19.
51. Spencer, S.L., Cappell, S.D., Tsai, F.C., Overton, K.W., Wang, C.L. and Meyer, T. (2013) The proliferation-quiescence decision is controlled by a bifurcation in CDK2 activity at mitotic exit. *Cell*, **155**, 369-383.
52. Nishioka, K., Rice, J.C., Sarma, K., Erdjument-Bromage, H., Werner, J., Wang, Y., Chuikov, S., Valenzuela, P., Tempst, P., Steward, R. *et al.* (2002) PR-Set7 is a nucleosome-specific methyltransferase that modifies lysine 20 of histone H4 and is associated with silent chromatin. *Mol Cell*, **9**, 1201-1213.
53. Rice, J.C., Nishioka, K., Sarma, K., Steward, R., Reinberg, D. and Allis, C.D. (2002) Mitotic-specific methylation of histone H4 Lys 20 follows increased PR-Set7 expression and its localization to mitotic chromosomes. *Genes Dev*, **16**, 2225-2230.
54. Tardat, M., Murr, R., Herceg, Z., Sardet, C. and Julien, E. (2007) PR-Set7-dependent lysine methylation ensures genome replication and stability through S phase. *J Cell Biol*, **179**, 1413-1426.
55. Sugimoto, N., Maehara, K., Yoshida, K., Ohkawa, Y. and Fujita, M. (2018) Genome-wide analysis of the spatiotemporal regulation of firing and dormant replication origins in human cells. *Nucleic Acids Res*, **46**, 6683-6696.
56. Miotto, B., Ji, Z. and Struhl, K. (2016) Selectivity of ORC binding sites and the relation to replication timing, fragile sites, and deletions in cancers. *Proc Natl Acad Sci U S A*, **113**, E4810-4819.
57. Besnard, E., Babled, A., Lapasset, L., Milhavet, O., Parrinello, H., Dantec, C., Marin, J.M. and Lemaitre, J.M. (2012) Unraveling cell type-specific and reprogrammable human replication origin signatures associated with G-quadruplex consensus motifs. *Nat Struct Mol Biol*, **19**, 837-844.
58. Woodfine, K., Fiegler, H., Beare, D.M., Collins, J.E., McCann, O.T., Young, B.D., Debernardi, S., Mott, R., Dunham, I. and Carter, N.P. (2004) Replication timing of the human genome. *Hum Mol Genet*, **13**, 191-202.
59. Ritzi, M., Baack, M., Musahl, C., Romanowski, P., Laskey, R.A. and Knippers, R. (1998) Human minichromosome maintenance proteins and human origin recognition complex 2 protein on chromatin. *J Biol Chem*, **273**, 24543-24549.
60. Saha, P., Chen, J., Thome, K.C., Lawlis, S.J., Hou, Z.H., Hendricks, M., Parvin, J.D. and Dutta, A. (1998) Human CDC6/Cdc18 associates with Orc1 and cyclin-cdk and is

selectively eliminated from the nucleus at the onset of S phase. *Mol Cell Biol*, **18**, 2758-2767.

61. Chong, J.P., Hayashi, M.K., Simon, M.N., Xu, R.M. and Stillman, B. (2000) A double-hexamer archaeal minichromosome maintenance protein is an ATP-dependent DNA helicase. *Proc Natl Acad Sci U S A*, **97**, 1530-1535.
62. Fry, D.W., Harvey, P.J., Keller, P.R., Elliott, W.L., Meade, M., Trachet, E., Albassam, M., Zheng, X., Leopold, W.R., Pryer, N.K. *et al.* (2004) Specific inhibition of cyclin-dependent kinase 4/6 by PD 0332991 and associated antitumor activity in human tumor xenografts. *Mol Cancer Ther*, **3**, 1427-1438.
63. Scott, S.J., Suvarna, K.S. and D'Avino, P.P. (2020) Synchronization of human retinal pigment epithelial-1 cells in mitosis. *J Cell Sci*, **133**. jcs247940.
64. Gambus, A., Jones, R.C., Sanchez-Diaz, A., Kanemaki, M., van Deursen, F., Edmondson, R.D. and Labib, K. (2006) GINS maintains association of Cdc45 with MCM in replisome progression complexes at eukaryotic DNA replication forks. *Nat Cell Biol*, **8**, 358-366.
65. Moyer, S.E., Lewis, P.W. and Botchan, M.R. (2006) Isolation of the Cdc45/Mcm2-7/GINS (CMG) complex, a candidate for the eukaryotic DNA replication fork helicase. *Proc Natl Acad Sci U S A*, **103**, 10236-10241.
66. Ilves, I., Petojevic, T., Pesavento, J.J. and Botchan, M.R. (2010) Activation of the MCM2-7 helicase by association with Cdc45 and GINS proteins. *Mol Cell*, **37**, 247-258.
67. Pesavento, J.J., Yang, H., Kelleher, N.L. and Mizzen, C.A. (2008) Certain and progressive methylation of histone H4 at lysine 20 during the cell cycle. *Mol Cell Biol*, **28**, 468-486.
68. Ishimi, Y. (2018) Regulation of MCM2-7 function. *Genes Genet Syst*, **93**, 125-133.
69 Jørgensen, S., Elvers, I., Trelle, M.B., Menzel, T., Eskildsen, M., Jensen, O.N., Helleday, T., Helin, K. and Sørensen, C.S. (2007) The histone methyltransferase SET8 is required for S-phase progression. *J Cell Biol*, **179**, 1337-1345.
70 Kent, L.N. and Leone, G. (2019) The broken cycle: E2F dysfunction in cancer. *Nat Rev Cancer*, **19**, 326-338.
71. Sherr, C.J. and McCormick, F. (2002) The RB and p53 pathways in cancer. *Cancer Cell*, **2**, 103-112.
72. Giacinti, C. and Giordano, A. (2006) RB and cell cycle progression. *Oncogene*, **25**, 5220-5227.

Figure Legends

Figure 1. Dynamics of Mcm3 based on immunostaining analysis.

A. Representative fluorescent images of Hoechst 33342, EdU, and Mcm3 in hTERT-RPE1 cells prepared by direct fixation (upper panels) or the pre-extraction method (lower panels). Bar, 20 μm. **B**. Single-cell plot analysis based on the images in **A**. The orange dots represent S-phase cells based on EdU intensities ($\log_2$(EdU) > -3). The number of cells examined in each panel is 400.

Figure 2. Dynamics of Mcm3 loading on chromatin during the cell cycle.

A. Mcm3 intensities plotted as a time course. The cells pulse-labeled with EdU for 30 min are incubated until the indicated times (upper bar) and applied to the single-cell plot analysis (lower panels). The orange dots represent S-phase cells at 0 h ($\log_2$(EdU) > -3). The number of cells examined in each panel is 400. **B**. Representative microscopic images of Cdt1 with Hoechst and Mcm3 staining. A closed arrowhead indicates a cell with high levels of both Cdt1 and Mcm3, and an open arrowhead indicates that a cell with high Mcm3 levels but low Cdt1 levels. Bar, 10 μm. **C**. Single-cell plot analysis based on the images in **B**. The pink dots represent G1-phase cells with high Cdt1 levels ($\log_2$(Cdt1) > 1.5 and Hoechst < 1.125). The number of cells examined in each panel is 400. The tick mark on the vertical axis of Mcm3 indicates a border between low and high levels.

Figure 3. Dynamics of Mcm3 in various cell lines.

A. Single-cell plot analysis of Mcm3 and EdU in HeLa, U2OS, MRC5, and IMR90 cells in the growth phase. The cells were pulse-labeled with EdU for 30 min and fixed at 0 h or 8 h later. The orange dots represent S-phase cells at 0 h ($\log_2$(EdU) > -3). The number of cells examined in each panel is 450. The tick mark on the vertical axis of Mcm3 indicates a border between low and high levels. **B**. Doubling times of HeLa, U2OS, hTERT-RPE1, MRC5, and IMR90 cells in the growth phase. The doubling time was determined from growth curves in five independent experiments. **C**. Duration for each phase of the cell cycle: G1 (low MCM, high MCM), S, G2 and M phases. Graphs on the top are examples of single-cell plot analysis in hTERT-RPE1 cells; magenta dots represent cells assigned for each of the phases indicated at the bottom. Estimation of duration of each cell cycle phase were described in Materials and Methods. The averages are plotted as bars and each data point (n = 5) are shown as open circles.

Figure 4. MCM dynamics under conditions of G1 arrest in hTERT-RPE1 cells. **A**. Representative microscopic images of Hoechst, Mcm2, histone H4K20me1, and EdU in hTERT-RPE1 cells under confluent conditions or treated with either Set8-siRNA or negative control-siRNA. Bar, 20 μm. **B**. Single-cell plot analysis based on **A**. Each dot represents the intensities of Mcm2, histone H4K20me1, and EdU in a single cell plotted against Hoechst 33342 intensities. The orange dots represent S-phase cells based on EdU intensities ($\log_2$(EdU) > -3) in siRNA (negative control). The tick mark on the vertical axis of Mcm2 indicates a border between low and high levels. The number of cells examined in each panel is 400. **C**. Genome-wide analysis of Mcm3 localization characterized using ChIP-seq. An example of chromosome 16: enrichment of Mcm3 obtained in this study is shown together with that of Orc2 (K562 cells;

GSM1717888), SNS (IMR-90 cells; GSM927235), and H4K20me1 (HeLa-S3 cells; GSM733689), and H3K9me3 (IMR90 cells; GSM1528890). Vertical axes are shown on the linear scale for Orc2 (RPKM_ChIP) and on the $\log_2$ scale for the others (RPKM_ChIP/RPKM_Input).

Figure 5. Identification of MCM hexamer states.

A. A schematic of MCM complex fractionation using the sucrose gradient ultracentrifugation method. **B**. Western blot analysis using a Mcm2 antibody following fractionation with a linear 5–30% sucrose gradient. The cells in the growth phase, under confluent conditions, and treated with Set8-siRNA were used. Molecular sizes derived from the sucrose gradient are indicated below the blots. **C**. Single-cell plot analysis of Mcm2 in the growth phase cells and palbociclib-treated cells. The tick mark on the vertical axis of Mcm2 indicates a border between low and high levels. The number of cells examined in each panel is 450. **D**. Western blot analysis using an Mcm2 antibody. The pellet fractions were prepared from the growth phase cells and 1 μM palbociclib-treated cells, followed by fractionation with sucrose gradient. **E**. Single-cell plot analysis of Cdc45, Mcm3, and EdU in hTERT-RPE1 cells in the growth phase. The orange dots represent the cells with high levels of Cdc45 ($\log_2$(Cdc45) > 0). The number of cells examined in each panel is 450. **F**. Western blot analysis using a Cdc45 antibody. The samples are the same as **D**.

Figure 6. The effect of siRNA-mediated depletion on Mcm2 and histone H4K20 methylation intensities. The cells were treated with siRNAs for 18 h and then pulse-labeled with EdU for 30 min. The cells were incubated until the indicated times (upper

bar) and applied to the single-cell plot analysis (lower panels). The orange dots represent S-phase cells at 0 h ($\log_2$(EdU) > -3). The blue dots at 8 h represent the cells newly entering the G1 phase (Hoechst < 1.125, $\log_2$(EdU) > 0, the squares in the EdU panels). The tick mark on the vertical axis of Mcm2 indicates a border between low and high levels. The number of cells examined in each panel is 450.

Figure 7. Relationship between histone H4K20 methylation levels and MCM hexamer states.

A. Representative microscopic images of Hoechst, H4K20me1, H4K20me2, and Mcm2. Bar, 20 μm. **B.** Single-cell plot analysis of H4K20me1, H4K20me2, and Mcm2. The G1 cells with high levels of H4K20me1 (Hoechst < 1.125 and $\log_2$(H4K20me1) > 0.3) are shown in light blue in the upper panel, those with low levels of H4K20me2 (Hoechst < 1.125 and $\log_2$(H4K20me2) < -0.1) in blue in the middle panel, and those with high levels of Mcm2 (Hoechst < 1.125 and $\log_2$(Mcm2) > 0.5) in pink in the lower panel. **C**. Scatter plots between H4K20me1 and Mcm2 intensities based on **B**. **D**. Single-cell plot analysis of Mcm2, H4K20me2, and H4K20me3 in cells treated with either control-siRNA, Set8-siRNA, or Suv420h1-siRNA. The tick mark on the vertical axis of Mcm2 indicates a border between low and high levels. The number of cells examined in each panel is 450.

Figure 8. A state model of the MCM hexamer during G1/S phases. The conversion of histone H4 methylation from mono to di/tri is a trigger for the transition from the single to double state of MCM hexamers. The cell cycle states of the cells used in this study are shown on right.

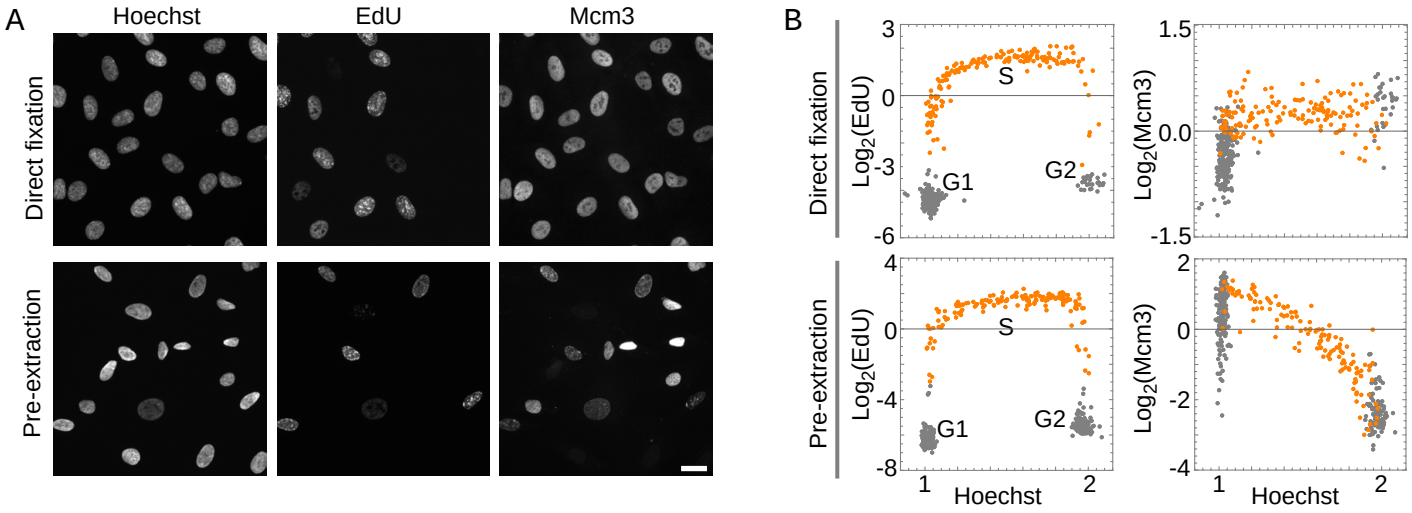

Figure 1

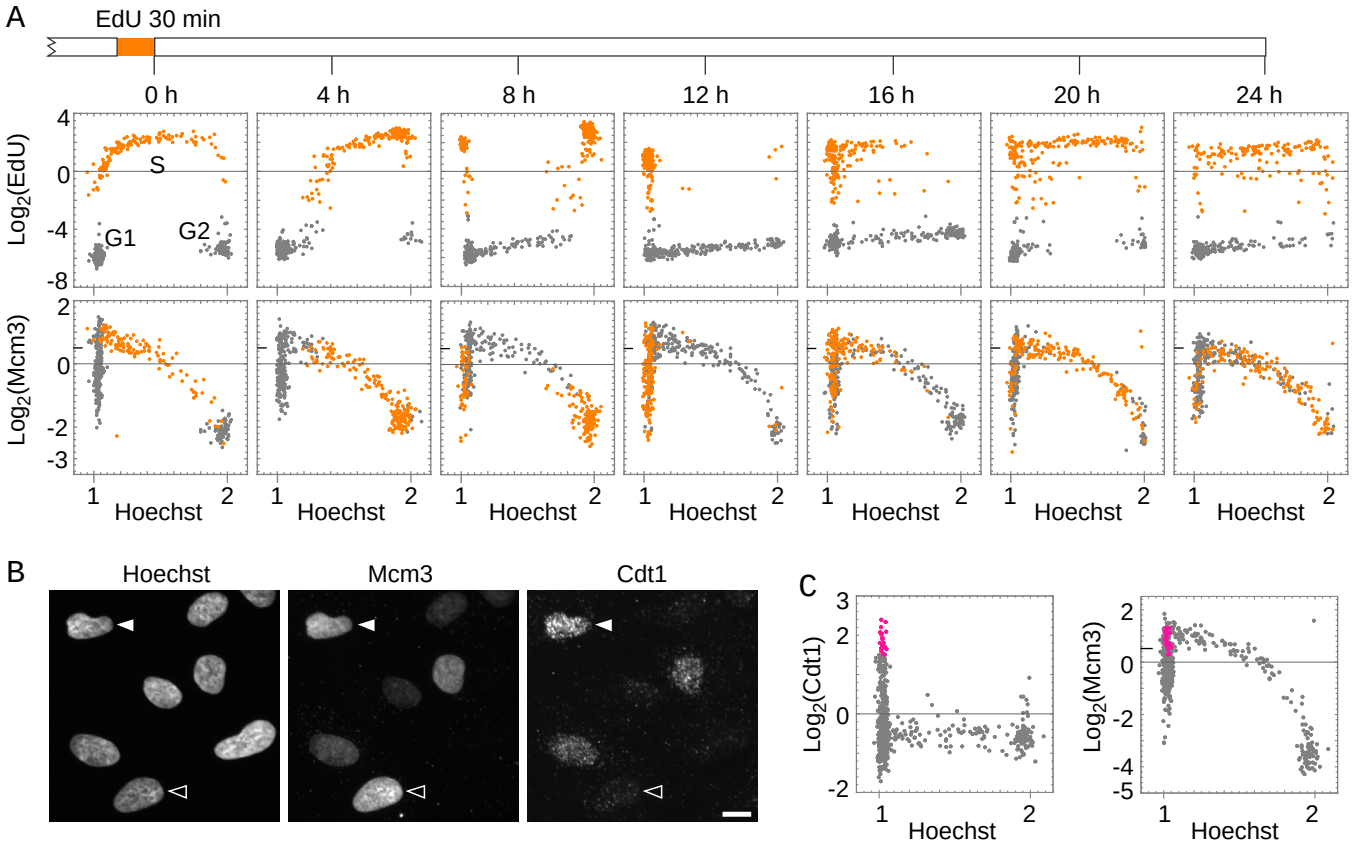

Figure 2

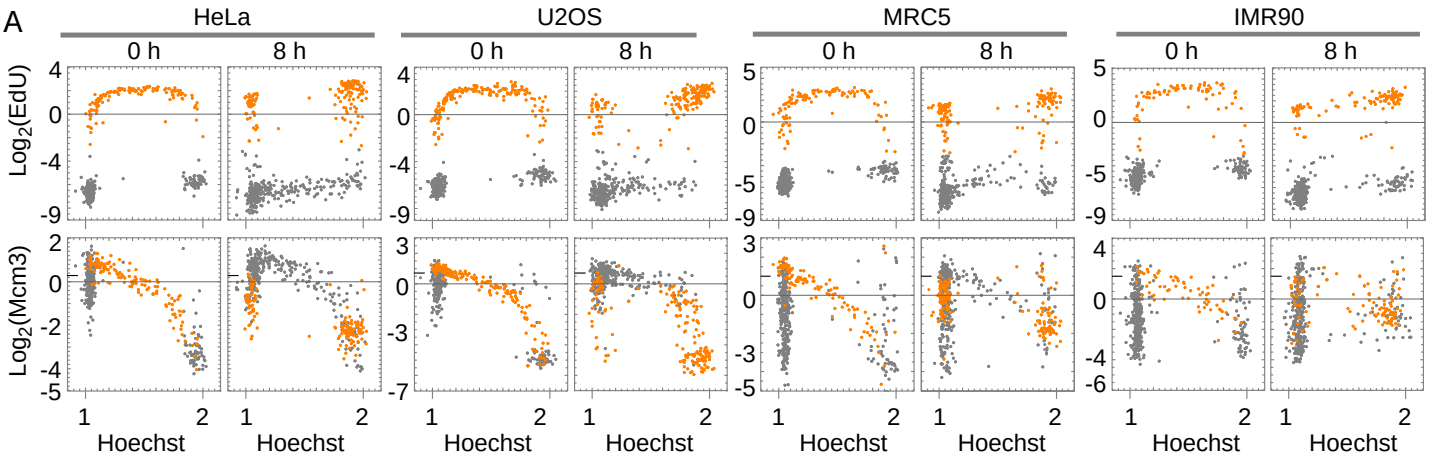

B

Doubling time

Cells	Average ± SD (h)
HeLa	20.4 ± 1.6
U2OS	24.9 ± 2.4
hTERT-RPE1	22.5 ± 1.2
MRC5	36.0 ± 5.7
IMR90	41.0 ± 2.9

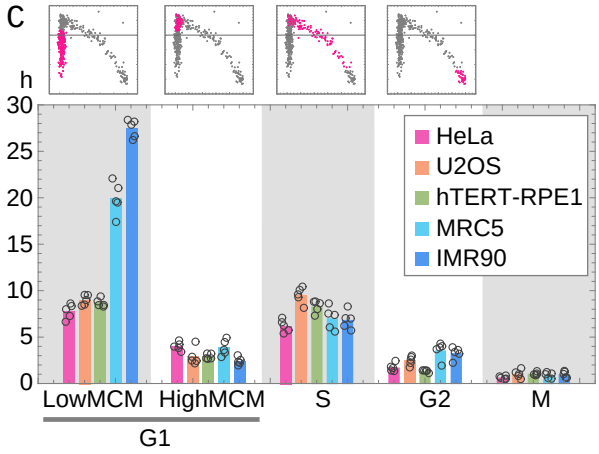

Figure 3

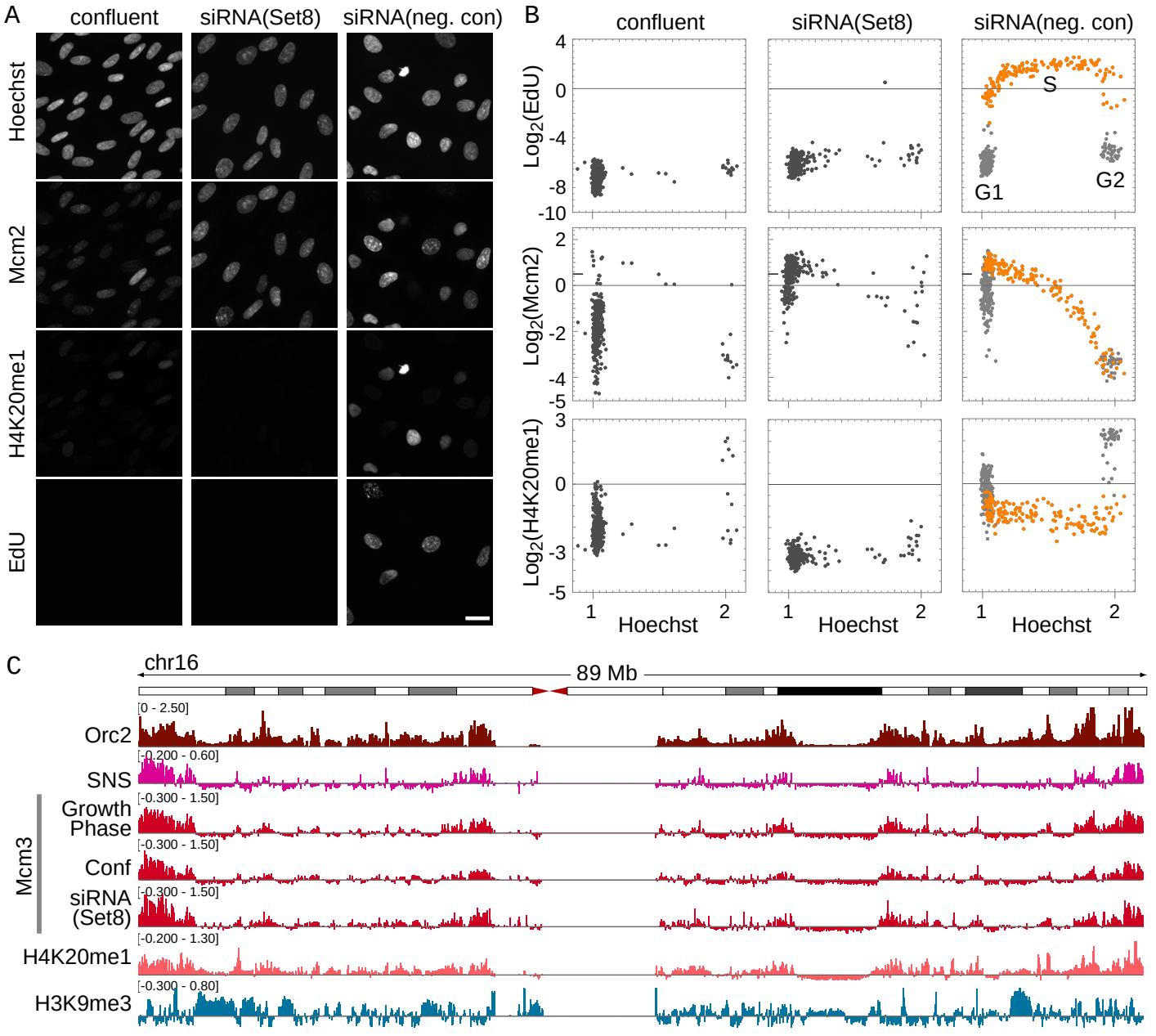

Figure 4

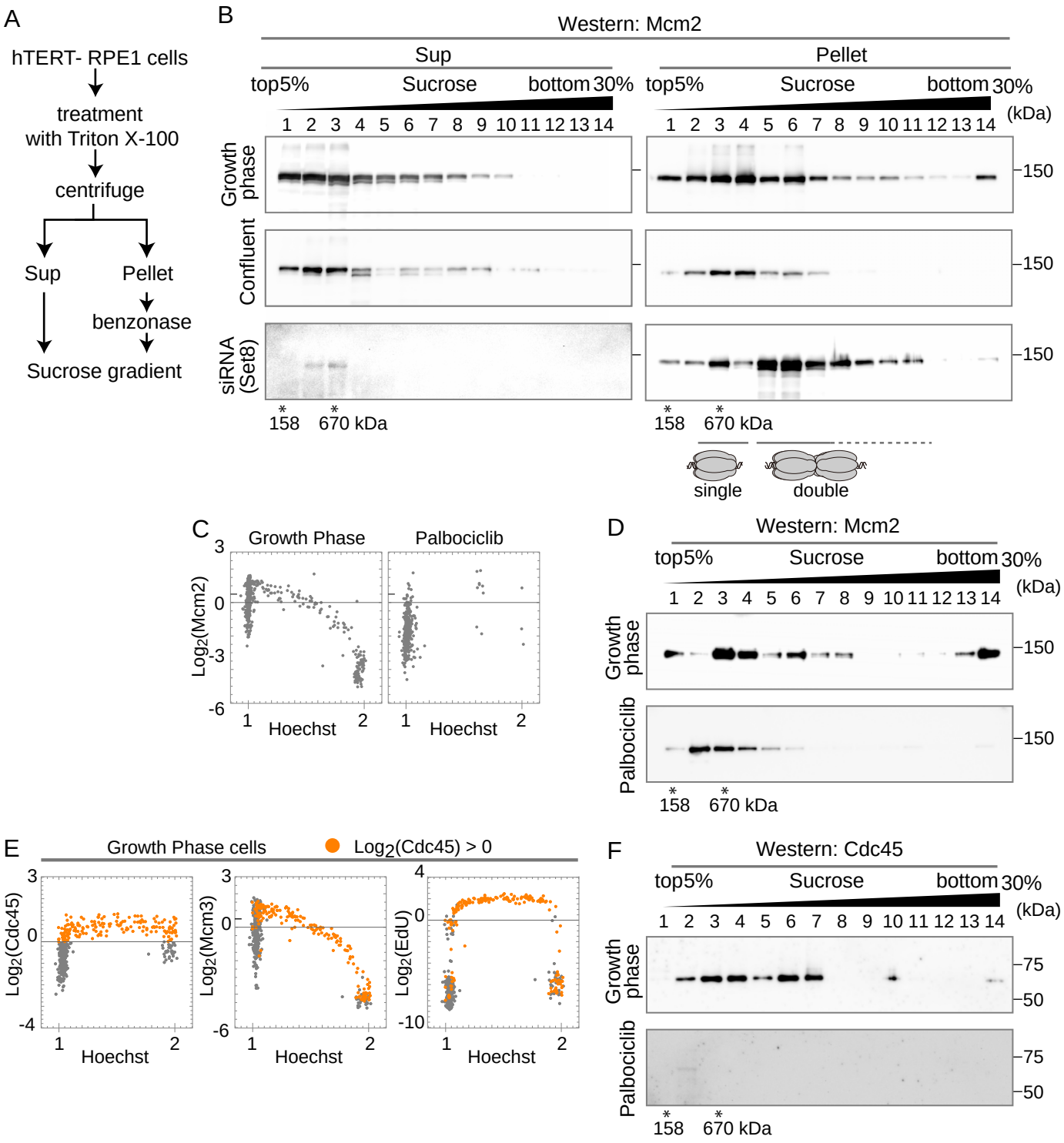

Figure 5

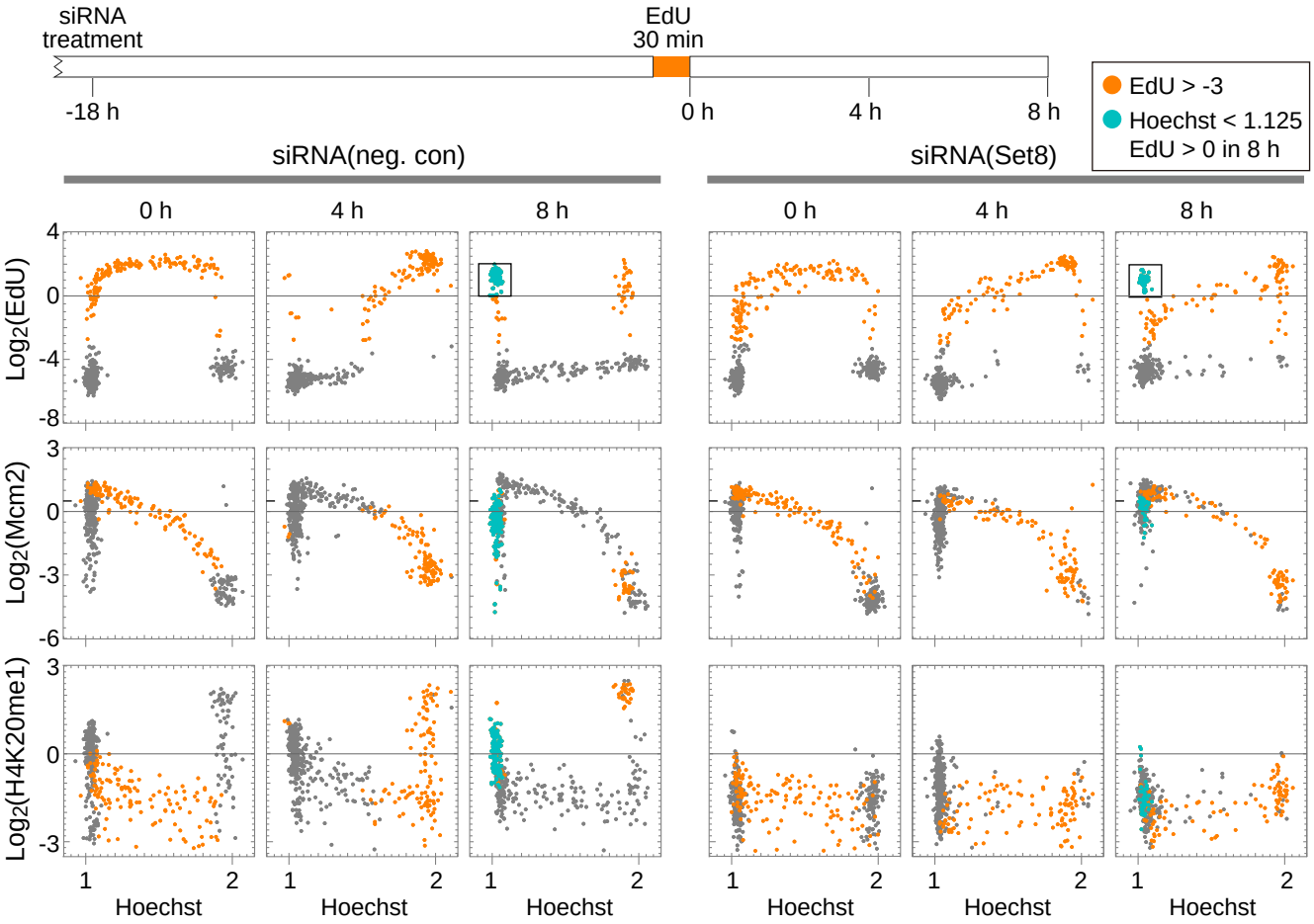

Figure 6

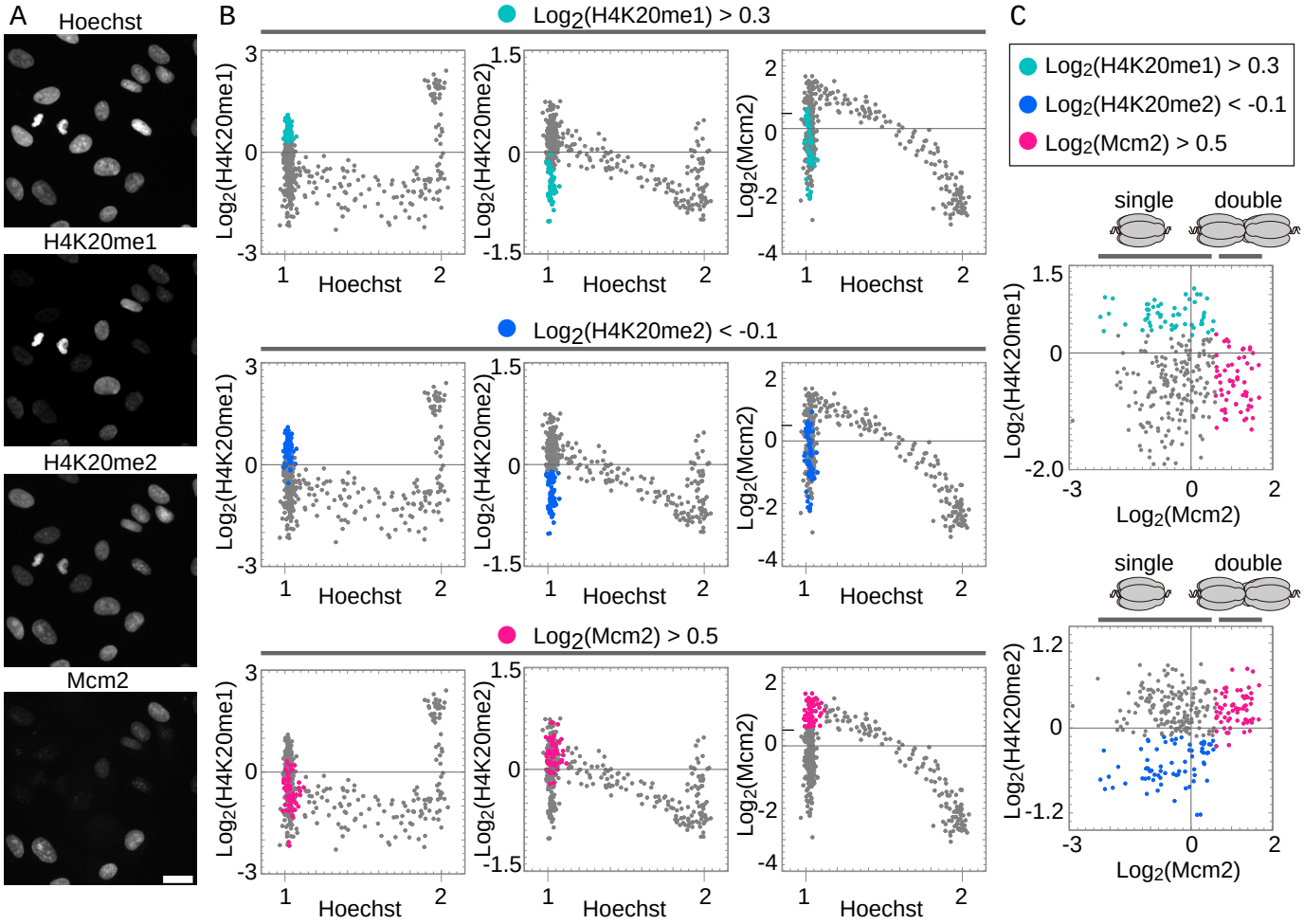

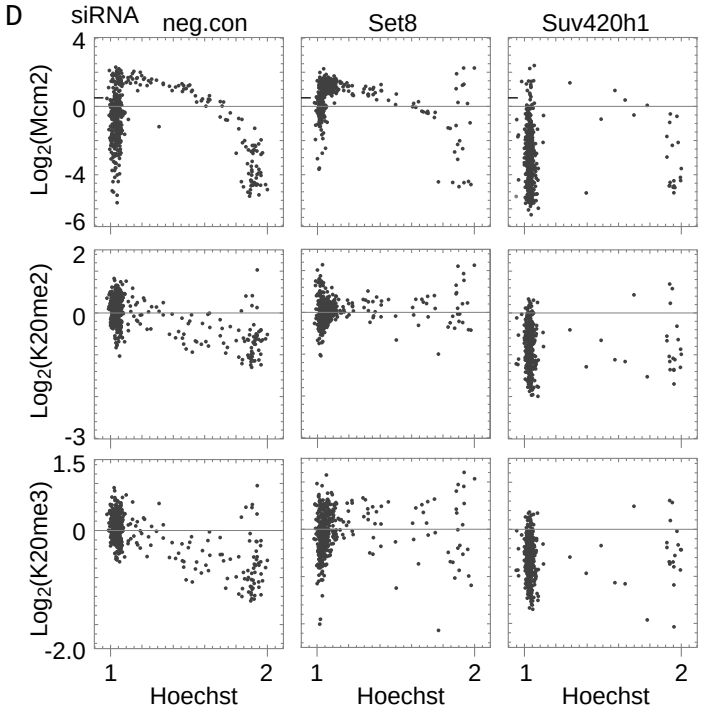

Figure 7

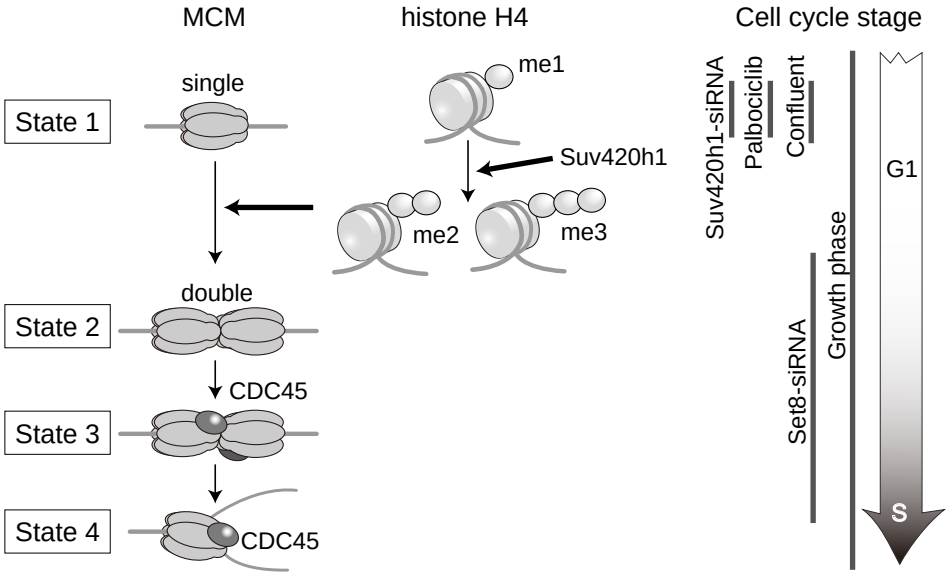

Figure 8